Calhoun: The NPS Institutional Archive

DSpace Repository

Faculty and Researchers | Faculty and Researchers' Publications

2017-05

Warm Layer and Cool Skin Corrections for Bulk Water Temperature Measurements for Air-Sea Interaction Studies

Alappattu, Denny P.; Wang, Qing; Yamaguchi, Ryan; Lind, Richard J.; Reynolds, Mike; Christman, Adam J.

Alappattu, Denny P., et al. "Warm layer and cool skin corrections for bulk water temperature measurements for airsea interaction Studies." Journal of Geophysical Research: Oceans (2017).
https://hdl.handle.net/10945/55114

This publication is a work of the U.S. Government as defined in Title 17, United States Code, Section 101. Copyright protection is not available for this work in the United States.

Downloaded from NPS Archive: Calhoun

http://www.nps.edu/library

Calhoun is the Naval Postgraduate School's public access digital repository for research materials and institutional publications created by the NPS community. Calhoun is named for Professor of Mathematics Guy K. Calhoun, NPS's first appointed -- and published -- scholarly author.

Dudley Knox Library / Naval Postgraduate School
411 Dyer Road / 1 University Circle
Monterey, California USA 93943

AGU PUBLICATIONS

JGR

Journal of Geophysical Research: Oceans

RESEARCH ARTICLE

10.1002/2017JC012688

Warm layer and cool skin corrections for bulk water temperature measurements for air-sea interaction studies

Denny P. Alappattu[1,2], Qing Wang[1], Ryan Yamaguchi[1], Richard J. Lind[1], Mike Reynolds[3], and Adam J. Christman[4]

[1]Department of Meteorology, Naval Postgraduate School, Monterey, California, USA, [2]Moss Landing Marine Laboratories, San Jose State University, Moss Landing, California, USA, [3]Remote Measurement and Research Co., Seattle, Washington, USA, [4]Department of Civil and Environmental Engineering and Earth Sciences, University of Notre Dame, Notre Dame, Indiana, USA

Key Points:
- Shipboard bulk and skin SST measurements were made from east coast of USA during CASPER-East field experiment
- Strong influence of wind speed, time of the day, and net longwave radiation flux on the bulk-skin temperature difference is noticed
- Bulk SST is corrected for cool skin, warm layer effects by quantifying the factors influencing bulk-skin SST difference

Correspondence to:
D. P. Alappattu,
dpalappa@nps.edu

Citation:
Alappattu, D. P., Q. Wang, R. Yamaguchi, R. J. Lind, M. Reynolds, and A. J. Christman (2017), Warm layer and cool skin corrections for bulk water temperature measurements for air-sea interaction studies, *J. Geophys. Res. Oceans*, *122*, 6470–6481, doi:10.1002/2017JC012688.

Received 9 JAN 2017
Accepted 19 MAY 2017
Accepted article online 24 MAY 2017
Published online 22 AUG 2017

Abstract The sea surface temperature (SST) relevant to air-sea interaction studies is the temperature immediately adjacent to the air, referred to as skin SST. Generally, SST measurements from ships and buoys are taken at depths varies from several centimeters to 5 m below the surface. These measurements, known as bulk SST, can differ from skin SST up to $O(1°C)$. Shipboard bulk and skin SST measurements were made during the Coupled Air-Sea Processes and Electromagnetic ducting Research east coast field campaign (CASPER-East). An Infrared SST Autonomous Radiometer (ISAR) recorded skin SST, while R/V Sharp's Surface Mapping System (SMS) provided bulk SST from 1 m water depth. Since the ISAR is sensitive to sea spray and rain, missing skin SST data occurred in these conditions. However, SMS measurement is less affected by adverse weather and provided continuous bulk SST measurements. It is desirable to correct the bulk SST to obtain a good representation of the skin SST, which is the objective of this research. Bulk-skin SST difference has been examined with respect to meteorological factors associated with cool skin and diurnal warm layers. Strong influences of wind speed, diurnal effects, and net longwave radiation flux on temperature difference are noticed. A three-step scheme is established to correct for wind effect, diurnal variability, and then for dependency on net longwave radiation flux. Scheme is tested and compared to existing correction schemes. This method is able to effectively compensate for multiple factors acting to modify bulk SST measurements over the range of conditions experienced during CASPER-East.

1. Introduction

Sea surface temperature (SST) is a fundamental parameter required for quantifying and modeling many important physical processes that take place at the ocean-atmosphere interface. The most important processes are exchanges of momentum, heat, and gases that are measured as surface layer fluxes. Accurate measurements of these fluxes are sensitive to SST measurement accuracy, which are often complicated by the method of observation. Research vessels and buoys conventionally make water temperature measurements from depths that generally vary from several centimeters to 5 m below the sea surface. These water temperatures below the air-sea interface are referred to as bulk SST. Skin SST, normally obtained using radiometric measurements at the infrared wavelength, is directly related to air-sea fluxes. This quantity must be used instead of bulk SST in the calculation of surface fluxes or to generate marine atmospheric surface layer (MASL) vertical profiles for optimal accuracy [e.g., *Alappattu et al.*, 2016]. Depending on measurement depth and prevailing conditions, the bulk and skin SSTs can differ anywhere from a few tens of a degree to $O(1°C)$ [*Minnett et al.*, 2011; *Gentemann and Minnett*, 2008; *Minnett*, 2003; *Donlon et al.*, 2002; *Fairall et al.*, 1996; *Schluessel et al.*, 1990].

The difference between the skin and bulk SSTs is caused by two known processes: the warm layer and the cool skin effects [*Minnett et al.*, 2011; *Minnett*, 2003; *Donlon et al.*, 2002; *Fairall et al.*, 1996]. Bulk SST measurements must be adjusted for both of these effects to achieve accurate surface flux calculations [*Fairall et al.*, 1996, 2003]. Previous studies have shown that failure to account for differences in the bulk and skin SST can lead to significant errors in many calculations, such as the estimation of evaporation duct height [*Frederickson et al.*, 1994], the global heat balance [*Lukas*, 1989; *Zeng and Dickinson*, 1998], and marine CO_2 fluxes [*Robertson and Watson*, 1992]. Quality skin SST measurements are also imperative to establish the accuracy of satellite SST observations [*Donlon et al.*, 2002].

© 2017. American Geophysical Union. All Rights Reserved.

Skin SST is normally derived from infrared radiometric measurements. The downward looking IR radiometer detects radiance having its origin on the thermal skin layer of the ocean. Such radiometers are not a standard component of ship or buoy-based measurements because deployment and frequent maintenance of any optical instruments, especially in a marine environment, becomes both difficult and costly. In addition, radiometric skin SST measurements are sensitive to rain and aerosols (mainly sea spray), which results in erroneous skin SST data under rainy and severe sea spray conditions.

Extensive measurements of bulk and radiometric skin SSTs were made during the Coupled Air-Sea Processes and Electromagnetic (EM) ducting Research East coast (CASPER-East) field campaign conducted offshore Duck, North Carolina. However, due to frequent rain and heavy sea spray conditions, radiometric skin SST data measured during the CASPER-East were not continuous. On the other hand, bulk SST measurements were more complete with minimal missing data compared to skin SST. The objective of this study is to obtain accurate SST data to represent the skin temperature, which is needed as input to evaporation duct models, from bulk SST obtained during the CASPER-East experiment. To accomplish this, a three-step correction scheme is developed based on wind speed, local time of observation, and net longwave radiation flux. Results derived from this correction scheme will be compared to those from the warm layer and cool skin correction in the Coupled Ocean Atmosphere Response Experiment (COARE) surface flux scheme and from the wind speed-based parameterizations proposed by *Donlon et al*. [2002] and *Minnett et al*. [2011]. The applicability of this empirical correction to other data sets will be discussed.

Section 2 will review the physical mechanisms contributing to the difference between the bulk and skin SSTs. CASPER field measurements will be discussed in section 3. Section 4 gives a comprehensive description of the development of the bulk SST correction scheme. A comparison of the bulk correction scheme with results from the models is given in section 5. A summary and conclusion follows in section 6.

2. Warm Layer and Cool Skin Effects

Fairall et al. [1996] and *Saunders* [1967] provide summaries of the physical basis of the warm layer and cool skin effects. The cool skin layer of the ocean is produced by the combined cooling effects of net longwave radiation, sensible heat flux, and latent heat flux. The surface skin layer of the ocean, much less than 1 mm thick [*Minnett*, 2011; *Hanafin*, 2002; *Hanafin and Minnett*, 2001; *Fairall et al*., 1996], is nearly always cooler than the underlying water because heat flux is generally directed outward from the ocean to atmosphere. The warm layer is a region in the upper few meters of the ocean where absorption of solar radiation causes considerable warming relative to the deeper mixed layer. Warm layers occur during the day when temperature stratification caused by the absorption of solar radiation is sufficiently strong to suppress shear-induced mixing from below. Thus, the warm layer is a diurnal phenomenon with effects that depend on the depth of the bulk SST measurement when there is a near-surface temperature gradient [*Minnett et al*., 2011; *Fairall et al*., 1996; *Schluessel et al*., 1990]. The bulk-skin SST difference is a combination of this cool skin effect and diurnal warming of the upper ocean resulting in the warm layer.

Numerous studies have attempted to model the cool skin and warm layer effects over the oceans [*Fairall et al*., 1996; *Saunders*, 1967; *Zeng et al*., 1999]. A simple physical model quantifying the bulk-skin temperature difference was first proposed by *Saunders* [1967]. *Fairall et al*. [1996] modified the parameterization by Saunders using bulk and skin SST observations from the western Pacific warm pool. In addition to this, parameterizations for the bulk-skin SST difference based solely on wind speed have also been developed [e.g., *Donlon et al*., 2002; *Minnett et al*., 2011].

Some studies classify surface temperatures as skin, subskin, and depth measurements. In this context, subskin is a laminar sublayer below the skin and the depth measurement is similar to the bulk measurement with its depth specified [*Donlon et al*., 2007]. Knowing the bulk measurement depth is beneficial when accounting for the vertical distribution of solar heating in the upper ocean. In our study here, we follow *Minnett et al*. [2011] and *Wilson et al*. [2013] to define the bulk-skin SST difference (ΔT_{obs}) as the difference between bulk SST (T_b) and the skin SST (T_s),

$$\Delta T_{obs} = T_b - T_s. \quad (1)$$

3. Experiment and Data

The CASPER-East field experiment was conducted in the coastal waters (within ~100 km from coast) near Duck, North Carolina (NC) from 10 October to 6 November 2015. Major objectives of the experiment are to investigate the role of coupled air-sea interaction processes on boundary layer thermodynamic gradients and to study the atmospheric effects on radio frequency (RF) propagation in the coastal environment. Measurements were made from multiple platforms including two research vessels, two research aircrafts, and a shore site at Duck, NC [*Wang et al*., 2015]. The research vessels that participated in the measurements were R/V *Hugh R. Sharp* (hereinafter *Sharp*) and R/V *Atlantic Explorer* (hereinafter *Explorer*). The primary data sets of bulk and skin SST used in this analysis were collected from *Sharp*. Figure 1 shows the area of the field experiment with the blue curve showing the cruise track of *Sharp* and the red dot indicating the location of Duck, NC.

Skin SST measurements were made using an absolute radiometric skin temperature probe, the Integrated Infrared SST Autonomous Radiometer (ISAR). The ISAR contains a single channel radiometer (9.6–11.5 μm spectral band pass), two blackbody reference cavities, and a rotating gold mirror [*Donlon et al*., 2008]. The gold mirror reflects incoming infrared radiation into the radiometer and rotates to point at the sea surface, sky, and blackbodies at various times. Correcting for reflected sky radiance and utilizing a single self-calibrating radiometer design, the ISAR is capable of measuring in situ sea surface skin temperature to an accuracy of 0.1 K. During CASPER-East, the ISAR was mounted on the port rail above the *Sharp* bridge. A major advantage of ISAR over other infrared radiometers is its capability to automatically close a shutter that protects its optical components from detected rain and sea spray. Therefore, a dedicated instrument operator is not required to manually protect the ISAR from severe and damaging weather conditions [*Donlon et al*., 2008]. Several periods of rain and sea spray occurred during the CASPER-East field experiment and skin SST measurements during these periods are not available. The ISAR data were postprocessed to have a nominal 3 min time resolution and was then averaged to produce SST at 10 min time interval.

Bulk SST data used in this analysis are made by *Sharp's* Surface Mapping System (SMS). The ship intake for bulk SST measurements from the *Sharp* is located 1 m below the mean ship waterline. In addition to bulk SST, SMS also records navigation, meteorological and surface data with a time resolution of 10 s. Unlike radiometric measurements, SMS measurements were made continuously through the storm days. Hence, the bulk SST measurements are more complete with minimal missing data compared to ISAR measurements. Wind measurements were collected from a sonic anemometer mounted approximately 12 m above sea level (ASL) on the *Sharp's* forward meteorological mast. Wind speed and direction are corrected for ship motion and orientation. Strict quality control is applied to the selection of *Sharp* data for the analysis. Only data corresponding to the wind direction within ±30° from the ship's heading are taken into account. Furthermore, data during periods when the ship made sudden maneuvers were eliminated from the data set.

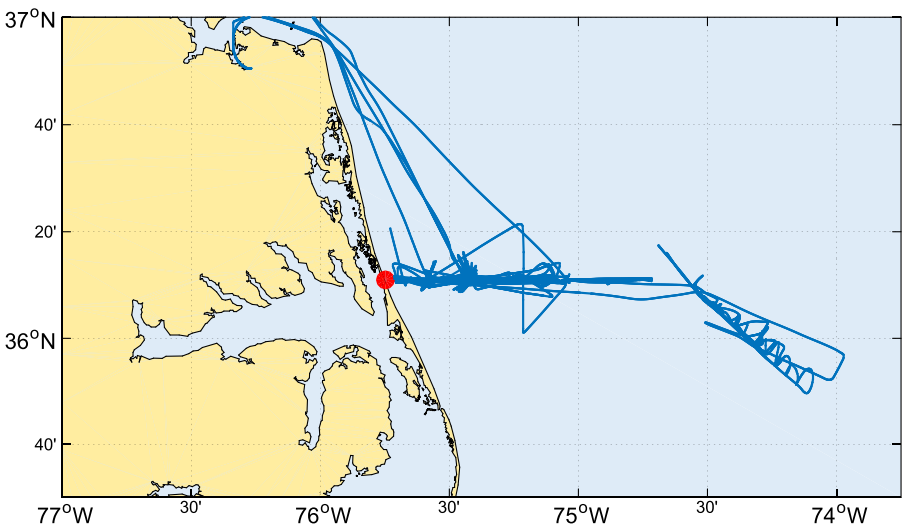

Figure 1. Region of CASPER-East field campaign overlaid with *Sharp* cruise track. Location of Duck, North Carolina is shown by red dot.

A final manual screening was performed to remove remaining obviously spurious data, resulting in 2123 quality-controlled data points for further analysis.

In addition to these data sets, shortwave and longwave net radiation data are used to model the cool skin and warm layer effect following *Fairall et al*. [1996]. Since no broadband radiation measurements were available onboard *Sharp*, the shortwave and longwave net radiation data were from the *Explorer* which was making synchronized measurements with *Sharp*. During CASPER-East measurements, the ships were normally within ~50 km from each other. Hence, it is assumed that the net radiation flux observed at the *Explorer* is comparable to that at *Sharp*. During CASPER-East, daylight saving time ended on 1 November 2015 near the end of the field campaign. Eastern Daylight Time (EDT) represents local time, which is 4 h behind Coordinated Universal Time (UTC). For reference, sunrise and sunset on 20 October 2015 at Duck, NC was at 0714 EDT and 1821 EDT, respectively. When working with the diurnal variation of the bulk-skin SST difference, we will use the EDT as the local time.

The next section will describe the procedure used to quantify upper ocean processes affecting observed bulk temperature during CASPER-East field experiment.

4. Variability of ΔT_{obs}

Figure 2a shows the quality controlled bulk (blue dots) and skin (red dots) SST data sampled during the entire period of CASPER-East. Most of the time during CASPER-East, bulk SST was higher than skin SST, indicating the overwhelming cool skin effects. During the period from 29 October to 2 November, measurements were made in the western boundary of the Gulf Stream (GS) and, as expected, SST in this region was highly variable with warm SST reaching 26°C on the GS side. The abrupt changes in SST in the GS region during this period resulted from measurements crossing the GS boundary. Observed bulk-skin SST differences (ΔT_{obs}) are shown in Figure 2b. ΔT_{obs} ranges from −0.5 to 1.2°C. An empirical probability distribution of the ΔT_{obs} variability is given in Figure 3. Approximately 73% of ΔT_{obs} are between 0.1 and 0.5°C (Figure

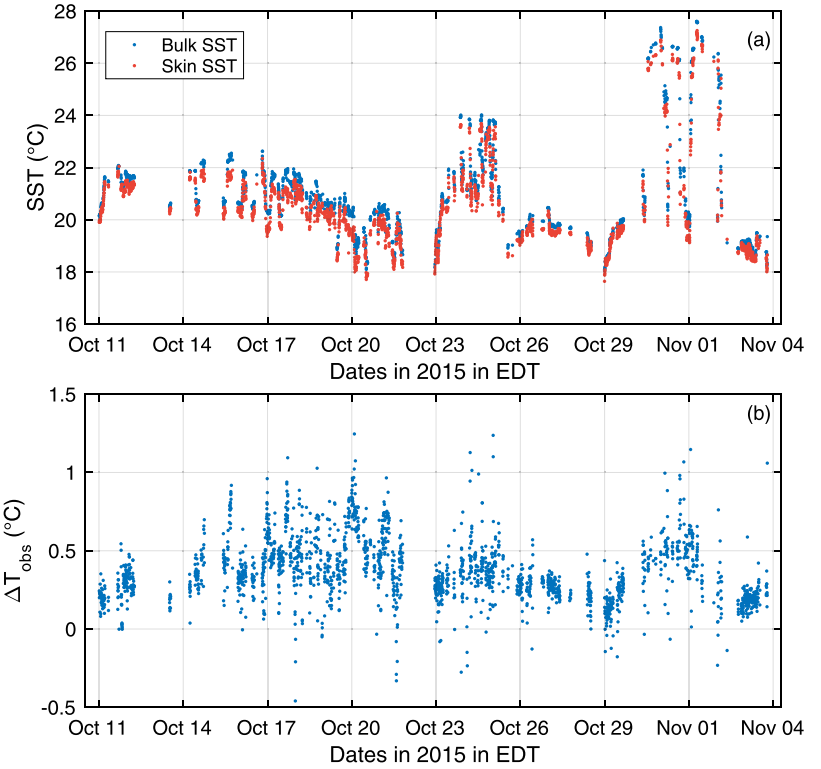

Figure 2. Time series of (a) bulk SST and radiometric skin SST and (b) bulk-skin SST difference (ΔT_{obs}) from CASPER-East measurements. Data gaps in time series are either due to the data loss in skin SST measurements or removal of data based on quality control criteria.

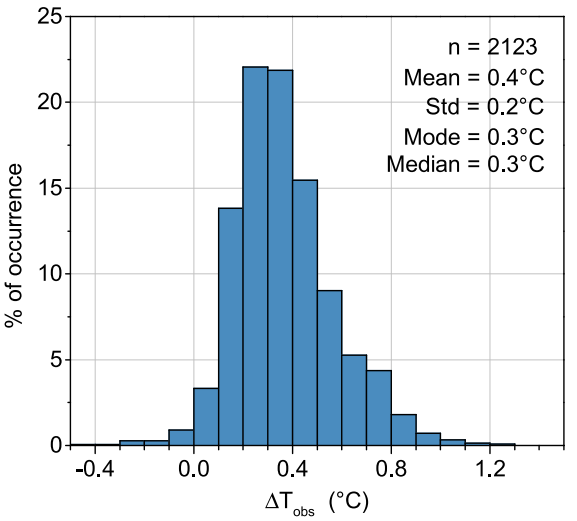

Figure 3. Empirical probability distribution of bulk-skin SST difference (ΔT_{obs}).

3), and roughly 23% of ΔT_{obs} are greater than 0.5°C. Negative ΔT_{obs} constitutes only 1.5% of the data. Mean bulk-skin SST is 0.4°C with a standard deviation of 0.2°C.

4.1. Physical Properties Affecting Variability of ΔT_{obs}

Using the observations from the Atlantic Ocean, *Donlon and Robinson* [1997] have provided a detailed study on the relationship of bulk-skin SST difference with various atmospheric and oceanic parameters. While analyzing the relationship of ΔT_{obs} with net surface heat flux and net longwave radiation, they noticed that clear-sky conditions produces largest ΔT_{obs}. Nevertheless, *Donlon and Robinson* [1997] identify wind speed as the key variable that controls the characteristics of ΔT_{obs} [*Donlon and Robinson*, 1997]. Observations from other oceanic regions also have confirmed the strong links between wind speed and ΔT_{obs} [e.g., *Minnett*, 2003; *Minnett et al*., 2011; *Horrocks et al*., 2003; *Donlon et al*., 2002]. A similar analysis using our data also showed strong dependence of bulk-skin SST difference on wind speed. Our study also reveals that, in addition to wind speed, the diurnal effects and net longwave radiation flux are also important factors in determining the variability of ΔT_{obs}.

Variability of ΔT_{obs} with respect to wind speed and local time are shown in Figure 4. Higher (>0.5°C) ΔT_{obs} occur predominantly when the wind speed is less than ~4 m s^{-1}. ΔT_{obs} tends to be less than 0.5°C for higher wind speeds. For low wind speed (<~4 m s^{-1}) cases, variability of ΔT_{obs} shows a clear diurnal signature. When winds are below 4 m s^{-1}, ΔT_{obs} in excess of 0.5°C occur only before sunrise and after ~1500 EDT. Higher ΔT_{obs} occur only when winds are less than 1–1.5 m s^{-1}. As mentioned before, ΔT_{obs} was generally positive during CASPER with the skin SST cooler than bulk SST, even during daytime.

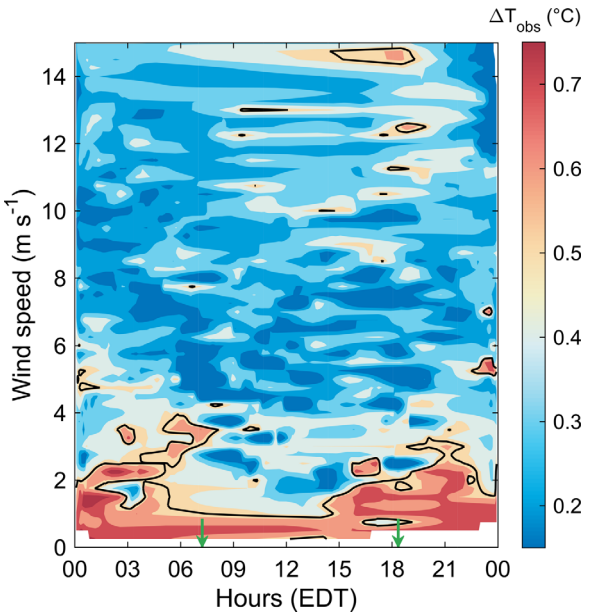

Figure 4. Variability of ΔT_{obs} with respect to local time (EDT) of observation and wind speed. The two green arrows denote sunrise and sunset times.

The dependence of bulk-skin SST difference on wind speed and local time of the day is consistent with the role of wind and solar radiation in generating upper ocean mixing and regulating ocean mixed-layer temperature. Wind forcing results in mechanical turbulence in the ocean mixed layer. This mixing effectively reduces the temperature difference at the skin and below the cool skin layer. Solar radiation tends to stabilize the upper ocean and hence reduce mixing. Solar radiation also increases the temperature of all layers of the upper ocean. Figure 4 suggests that the amount of shortwave radiation absorbed within the mixed layer is insufficient to overcome cooling from sensible, latent, and longwave fluxes [*Ward*, 2006]. However, absorption of the shortwave radiation during daytime effectively resulted in a reduction in bulk-skin SST difference during the day. This is the reason for diurnal variability of ΔT_{obs} in Figure 4. Apparently, in the CASPER-East cases, wind speed exceeding 4 m s^{-1} introduced sufficient turbulent

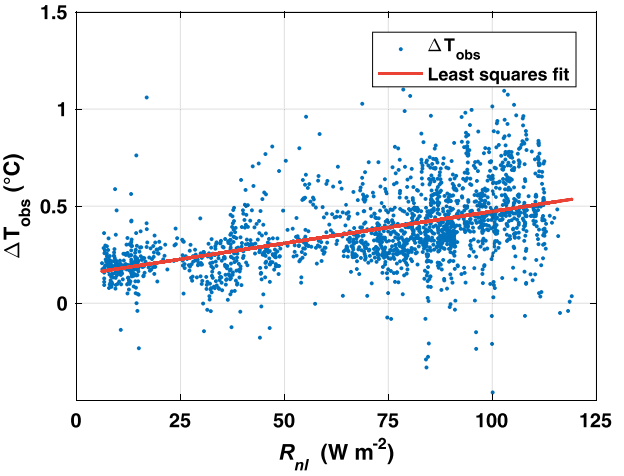

Figure 5. Scatterplot between net longwave radiation flux and ΔT_{obs}.

mixing to the upper ocean to reduce the solar radiation effect through mixing in a deeper layer and possibly through cooling as a result of entrainment at the base of the ocean mixed layer. Hence, when winds were relatively strong, the diurnal variation of the bulk-skin SST difference is not apparent.

Scatterplot of net longwave radiation versus the ΔT_{obs} is shown in Figure 5 (blue dots). It can be seen that, bulk-skin SST difference increases with net longwave radiation flux. Occurrence of higher (>0.5°C) ΔT_{obs} increases considerably for R_{nl} values higher than ~80 W m^{-2}. Linear fit to the data is shown by red line (Figure 5). Increase in net longwave radiation flux results in enhanced radiative cooling of the ocean surface. This leads to further reduction in skin SST thereby increasing the bulk-skin SST difference.

The bulk SST correction scheme to be discussed below is based on the findings of wind, local time, and net longwave flux dependence shown in Figures 4 and 5. Since ΔT_{obs} is dependent on wind speed and at low wind speeds displays diurnal variability, it is categorized as either a low wind (<4 m s^{-1}) or high wind (>4 m s^{-1}) observation, denoted as ΔT_l and ΔT_h, respectively, and defined as

$$\Delta T_l = T_{bl} - T_{sl}, \tag{2}$$

and

$$\Delta T_h = T_{bh} - T_{sh}, \tag{3}$$

where T_{bl} (T_{bh}) and T_{sl} (T_{sh}) are, respectively, the bulk and skin SST observations corresponding to low wind speeds (high wind speeds).

Figure 6 shows the variability of 2 h bin-averaged ΔT_l (blue curve) and ΔT_h (red curve) with respect to local time. Error bars represent one standard deviation estimated for each bin. The diurnal variability of ΔT_l is clear in this figure (blue curve). The average ΔT_l is lower during the daytime between ~0700 EDT and ~1500 EDT in comparison with the rest of the period. Peak to peak amplitude of the diurnal signal observed in ΔT_l was 0.3°C. Notable is the absence of a diurnal signal in ΔT_h (red curve). Based on these observations, ΔT_l is quantified first with respect to wind speed, and second, with respect to the local time of observation. Since the high wind cases were independent of diurnal variability, quantification for wind speed dependence should be sufficient for ΔT_h.

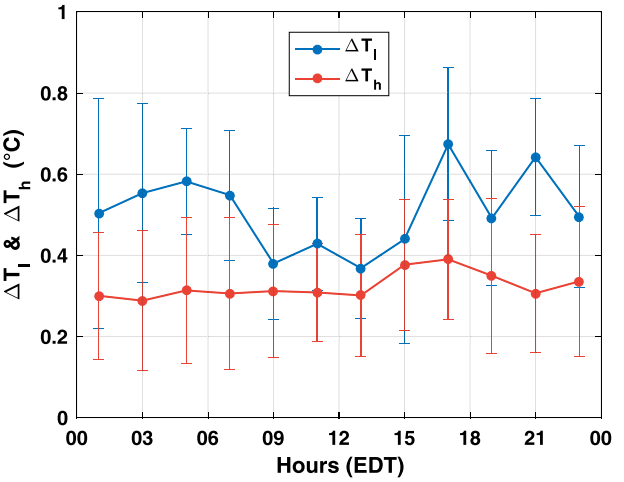

Figure 6. Variability of 2 h bin-averaged ΔT_l and ΔT_h with respect to local time (EDT).

4.2. ΔT Correction Based on Wind Speed

Dependence of ΔT_l on wind speed is shown in Figure 7a, with a clear trend of decreasing ΔT_l with increasing wind. A quadratic least squares fit is applied to

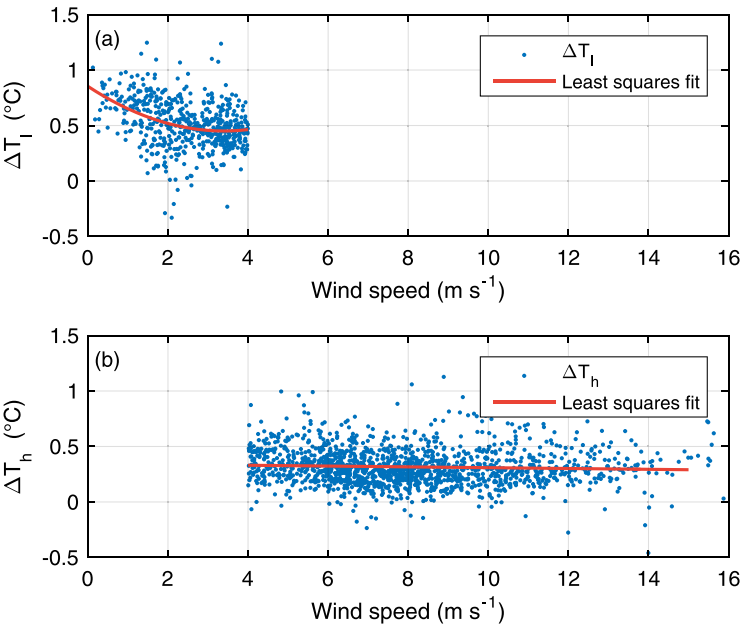

Figure 7. Wind speed dependence of (a) ΔT_l and (b) ΔT_h.

the observations and shown as a red line. Wind speed (U) dependence of temperature difference for low winds can be represented by a quadratic equation of the form

$$\Delta T_{l\_w} = aU^2 + bU + c, \quad (4)$$

where $a = 0.035\ \mathrm{m^{-2}\ s^2\ ^\circ C}$, $b = -0.24\ \mathrm{m^{-1}\ s\ ^\circ C}$, and $c = 0.85^\circ\mathrm{C}$.

Above 4 m s^{-1} ΔT_h shows a nearly linear relationship with wind speed (Figure 7b). The parameterization that best fits the SST measurements under these conditions is

$$\Delta T_{h\_w} = dU + e, \quad (5)$$

where $d = -0.0037\ \mathrm{m^{-1}\ s\ ^\circ C}$ and $e = 0.35^\circ\mathrm{C}$.

ΔT_l and ΔT_h variability are examined after applying the wind speed correction by subtracting the wind speed related temperature difference (ΔT_{l_w} and ΔT_{h_w}) from the corresponding bulk SST values (T_{bl} and T_{bh}). Bulk SST, after the wind-based correction for low winds, can be written as

$$T_{bl\_w} = T_{bl} - \Delta T_{l\_w}, \quad (6)$$

and for high winds is

$$T_{bh\_w} = T_{bh} - \Delta T_{h\_w}. \quad (7)$$

The resulting bulk-skin SST differences corresponding to low and high wind speeds after the first correction are

$$\Delta T_{l\_1} = T_{bl\_w} - T_{sl}, \quad (8)$$

and

$$\Delta T_{h\_1} = T_{bh\_w} - T_{sh}. \quad (9)$$

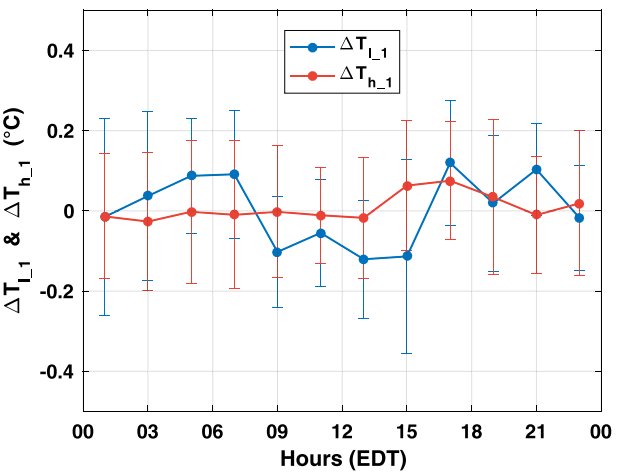

Figure 8. Variability of 2 h bin-averaged ΔT_{l_1} and ΔT_{h_1} with respect to local time (EDT).

Figure 8 shows 2 h bin-averaged ΔT_{l_1} and ΔT_{h_1} with respect to the hours of day in EDT. Error bars represent one standard deviation of the data in each 2 h bin. The wind-based correction significantly reduced the bias in temperature differences with the bin-averaged ΔT_{l_1} and ΔT_{h_1} closer to zero; however, a diurnal signal is still apparent in ΔT_{l_1}. Recalculated peak-to-peak amplitude of the diurnal signal is only reduced marginally by 0.06°C from its original value of 0.31°C. To remove the diurnal signal, ΔT_{l_1} variability is parameterized again based on the local time of observation.

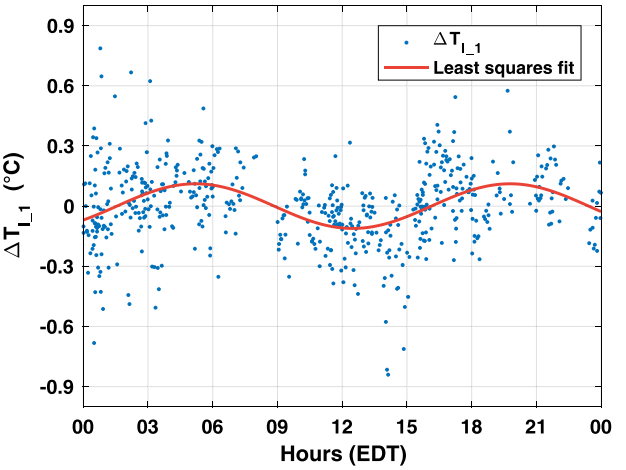

Figure 9. Variability of ΔT_{l_1} with respect to local time and sine fit.

4.3. ΔT Correction With Respect to Local Time

In Figure 9, the blue dots are the ΔT_{l_1} values were calculated as described in the previous section and a sinusoidal function best fits the diurnal variability of ΔT_{l_1}. The sine function fitted to the data, shown as red curve in Figure 9, is given by

$$\Delta T_{l\_d} = A \times \sin(\omega t + \varphi), \tag{10}$$

where t is the local time (EDT) of observation. Coefficients $A = 0.11^{\circ}$C, $\omega = 10.35\ s^{-1}$, and phase of the sine curve $\varphi = 0.67$.

Similar to equation (6), the bulk SST for low winds after the diurnal correction can be defined as

$$T_{bl\_d} = T_{bl\_w} - \Delta T_{l\_d}. \tag{11}$$

Note here that ΔT_{l_d} is subtracted from T_{bl_w}, which has been previously corrected for wind speed dependence. Finally, the temperature difference corresponding to low wind speeds after the second diurnal correction is

$$\Delta T_{l\_2} = T_{bl\_d} - T_{sl}. \tag{12}$$

The two-step correction results applied to the low wind case are shown in Figure 10. Two hour bin average and one standard deviation of the initial temperature difference (ΔT_l), temperature difference after first wind-based correction (ΔT_{l_1}), and corrected for diurnal signal (ΔT_{l_2}) are shown in blue, red, and green, respectively. The wind-based correction reduced the mean temperature difference from 0.5°C (mean of ΔT_l) to a value close to zero (mean of ΔT_{l_1}), but left the diurnal signal more or less the same (red curve). The second correction, based on the local time of observation, removed the remaining diurnal signal from the temperature difference data. As mentioned before, high wind cases are independent of diurnal variability. Hence, no diurnal corrections are applied for high wind cases. The composite of ΔT_{l_2} and ΔT_{h_1} is the bulk-skin SST difference after applying the corrections. We denote this composite temperature difference as ΔT_{wd}. Similarly, the composite of bulk SST corrected for wind speed and diurnal variability is denoted as T_{b_wd}, which is the composite of T_{bl_d} and T_{bh_w}.

4.4. ΔT Correction With Respect to Net Longwave Radiation Flux

In section 4.1, we discussed about the relationship between the net longwave radiation flux and the bulk-skin SST difference observed in the CASPER data (Figure 5). Now, the scatterplot in Figure 11a suggests that ΔT_{wd} (bulk-skin SST difference after applying the wind and diurnal corrections) also shows an increasing trend with net longwave radiation flux, even though above procedures considerably reduced the bias. A linear fit (red curve in Figure 11a) having the following form (equation (13)) is found to be optimum for representing the dependence of ΔT_{wd} variability on R_{nl}:

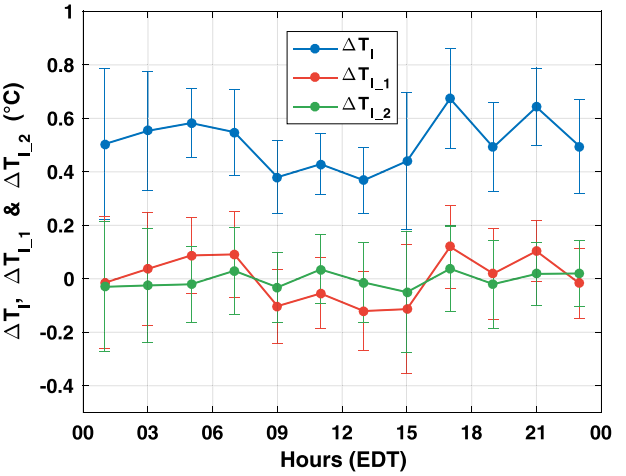

Figure 10. Variability of 2 h bin-averaged ΔT_l, ΔT_{l_1}, and ΔT_{l_2} with respect to local time (EDT).

$$\Delta T_r = f R_{nl} + g, \tag{13}$$

here $f = 0.002\ W^{-1}\ m^2\ ^{\circ}C$ and $g = -0.15^{\circ}$C.

Bulk SST after quantifying the ΔT_{wd} for its dependence on R_{nl} is given by,

$$T_{b\_cor} = T_{b\_wd} - \Delta T_r. \tag{14}$$

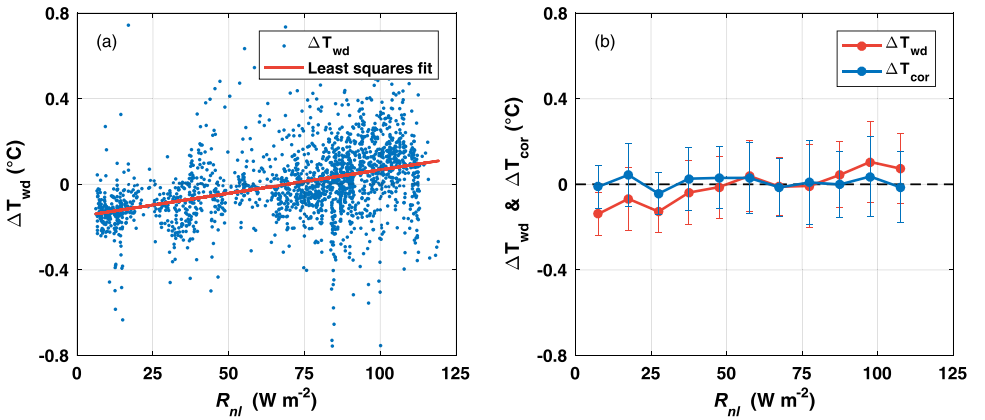

Figure 11. (a) Scatterplot between net longwave radiation flux and ΔT_{wd} and (b) variability of bin-averaged ΔT_{wd} and ΔT_{cor} with respect to net longwave radiation flux.

Corresponding bulk-skin SST differences can be written as,

$$\Delta T_{cor} = T_{b\_cor} - T_s. \tag{15}$$

In Figure 11b, bin average of the temperature difference after quantifying for the dependence on net longwave radiation (ΔT_{cor}) is shown in blue. Red curve is the bin average of ΔT_{wd}. Error bars are the one standard deviation of the data in each bin. It can be seen that, in comparison to the ΔT_{wd} (red curve), ΔT_{cor} (blue curve) lies close to the zero line. Moreover, ΔT_{cor} variability is independent of net longwave radiation flux.

Figure 12 shows the comparison between ΔT_{obs} and ΔT_{cor}. The red and blue curves in Figure 12a represent variability of ΔT_{obs} and ΔT_{cor}, respectively, versus local time and Figure 12b shows their variabilities with wind speed. It is evident from these figures that the three-step correction approach discussed here is effective at significantly reducing the difference between bulk and skin SSTs. Before correction, the mean of ΔT_{obs} was 0.4°C and following correction, the mean of ΔT_{cor} reduced almost to 0°C. This empirical method effectively adjusts *Sharp's* bulk SST data to a skin SST.

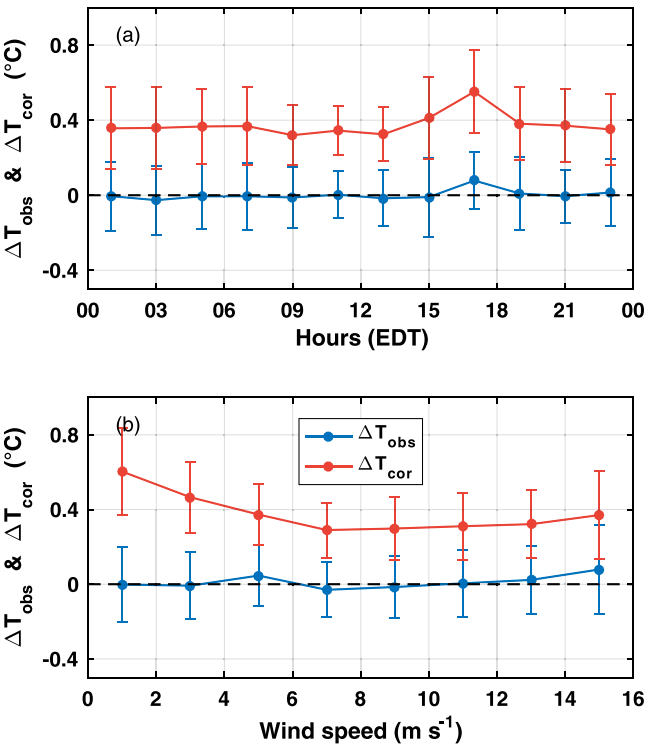

Figure 12. Variability of ΔT_{obs} and ΔT_{cor} (a) 2 h bin-averaged with respect to local time and (b) bin-averaged in 2 m s^{-1} with respect to wind speed.

Figure 13a is the scatterplot between radiometric skin SST (T_s) and observed bulk SST (T_b). Figure 13a shows data points above the red line representing a positive bias in bulk SST compared to the observed radiometric skin SST. Figures 3b and 3c show the scatterplot between T_{b_wd} versus T_s and T_{b_cor} versus T_s, respectively. In comparison to Figure 13a, data points lie along the 1:1 line in Figures 13b and 13c. This suggests that our method is efficient in removing the cool skin and warm layer effects from the bulk SST data. Moreover, it should be noted here that the no significant difference is noticed between Figures 13b and 13c. This is because the wind speed and diurnal corrections could able to reduce the

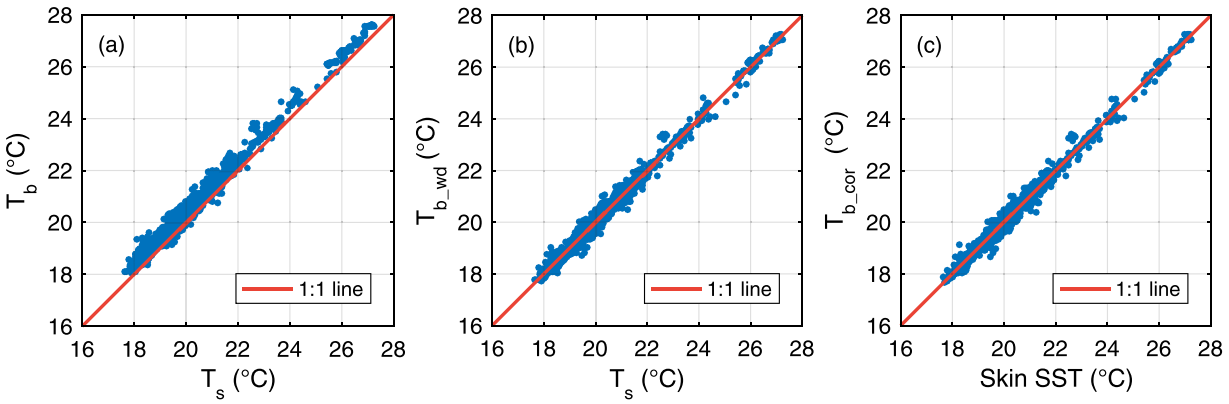

Figure 13. Scatterplot between skin SST and bulk SST (a) before correction (b) after correction for wind speed dependence and diurnal variability and (c) after final correction for dependence on net longwave radiation flux.

bulk-skin SST difference significantly. Therefore, in the absence of longwave radiation data, the wind speed and diurnal corrections applied to the bulk SST can provide a good approximation for skin SST.

5. Comparison With Models

In this section, model predictions for bulk-skin SST difference are compared using the data observed during the CASPER-East. Three models to be considered were discussed in *Fairall et al.* [1996, hereinafter FA-96], *Donlon et al.* [2002, hereinafter DN-02], and *Minnett et al.* [2011, hereinafter MN-11]. Models by DN-02 and MN-11 are similar and both assume an exponential dependence of bulk-skin SST difference (ΔT) on wind speed for wind speeds above 2 m s^{-1}. Their wind speed dependent functions have the following form:

$$\Delta T = a + b\ \exp\left(-\frac{U}{U_0}\right), \tag{16}$$

where U is the wind speed. In the DN-02 model, the coefficients a, b, and U_0 have values -0.14, 0.30, and 3.7, respectively, whereas MN-11 apply values 0.133, 0.637, and 3.279. In order to avoid diurnal warm layer effect, DN-02 considered only nighttime observations in their analyses.

In the FA-96 model, cool skin parameterization is based on the analysis by *Saunders* [1967]. Using dimensional arguments, *Saunders* [1967] presented a physical model for the cool skin effect given as

$$\Delta T = \frac{\lambda Q \nu}{k u_*}, \tag{17}$$

where Q is the net heat flux out of the ocean, ν is the kinematic viscosity of seawater, k is the thermal conductivity of seawater, u_* is the friction velocity in seawater, and λ is an empirical proportionality constant. According to *Saunders* [1967], λ can vary from 5 to 10. This model applies only to the forced convection regime, and in this regime ΔT is independent of wind speed. *Fairall et al.* [1996] modified the parameterization by *Saunders* [1967] in which λ varies as a function of heat flux and friction velocity, and provides a combined expression for ΔT applicable at all wind speeds. The diurnal heating model in FA-96 is based on the model proposed by *Price et al.* [1986]. This model determines diurnal warming as the summation of vertical mixing and radiation processes governed by local surface heat and momentum fluxes [*Niller and Kraus*, 1977; *Gentemann et al.*, 2009]. Cool skin and warm layer model, developed by FA-96, is included in the COARE 3.0 bulk flux algorithm [*Fairall et al.*, 2003]. In this analysis, the formulation in COARE 3.0 algorithm is used to model bulk-skin SST difference.

In Figure 14, gray dots represent the observed bulk-skin SST difference from CASPER-East observations as a function of wind speed. Bin averages of these data are shown as the black curve with error bars representing one standard deviation. The red curve is modeled ΔT using the FA-96 scheme. Bulk-skin SST difference from observations and FA-96 agree fairly well in the moderate wind regime between $\sim$3 and $\sim$7 m s^{-1}. For low winds ($<$3 m s^{-1}) the FA-96 model underestimates the bulk-skin SST difference, whereas for high winds ($>$7 m s^{-1}) the model overestimates the difference.

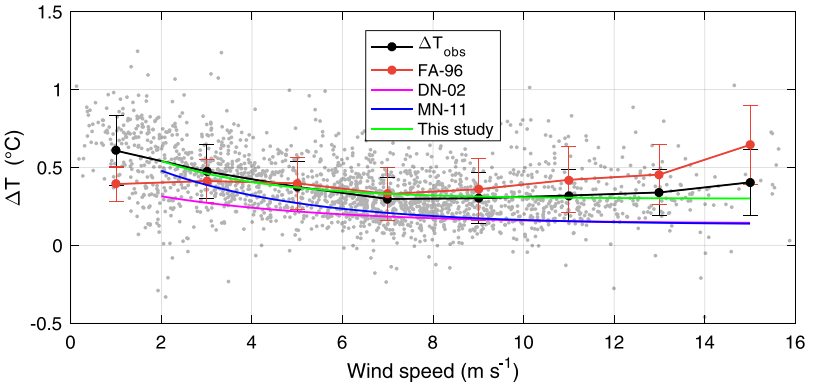

Figure 14. Comparison of observed bulk-skin SST difference using different correction models.

Figure 14 also shows that the wind speed-based parameterizations of DN-02 and MN-11 underestimate observed bulk-skin SST difference. As pointed out before, DN-02 and MN-11 assume an exponential dependence of ΔT on wind speed. A similar exponential fit applied to the CASPER data set is shown by the green curve, for which the coefficients a, b, and U_0 in equation (16) are found to be 0.30, 0.55, and 2.44, respectively. The exponential fit (green curve) matches well with the mean ΔT_{obs} (black curve) for wind speeds between 2 and 12 m s^{-1}. SST data used to model the bulk-skin SST difference reported by DN-02 and MN-11 were taken from observations in the open ocean and from different regions in the Pacific and Atlantic Oceans, whereas this study represents the variability of the bulk-skin SST difference in the coastal waters. Differences among CASPER-East observations and models based on the data from open ocean could be attributed to different wind conditions and boundary layer dynamics. Moreover, effects of river discharge on the bulk-skin SST difference in coastal regions cannot be ruled out. Further studies are planned that will incorporate more data from various coastal regions to understand the features of near-coastal bulk-skin SST difference and how they differ from open ocean estimates.

6. Summary

SST is a key parameter required for oceanographic, meteorological, and climatology applications. Accurate SST measurements are imperative for the correct estimation of many processes that take place near the ocean-atmosphere interface, such as surface layer fluxes. Conventional bulk SST measurements from research vessels and buoys are made from water depths that can vary from several centimeters to 5 m below the platform's mean water level. However, the skin SST at the air-sea interface is directly relevant to the air-sea flux exchange and has to be used in flux calculations instead of the bulk SST. Depending on the depth of the measurement, the bulk temperature can differ from the skin SST by a range between a few tens of a degree to O(1°C). This difference between the skin and bulk temperature is caused by two processes known as the warm layer and cool skin effects resulting from the absorption of insolation, heat exchange with the atmosphere, and subsurface turbulent mixing.

Shipboard measurements of bulk SST and skin SST were made during the CASPER-East field campaign conducted offshore Duck, North Carolina during October–November 2015. The surface mapping system of R/V *Hugh R. Sharp* provided bulk SST measurements. Seawater intake for the bulk SST was located 1 m below the ship mean water line. Skin SST measurements were collected using an ISAR. The ISAR did not take measurements under rain and/or sea-spray conditions and resulted in skin SST data loss during these periods. Bulk SST measurement were made continuously throughout the storms, hence bulk SST data are more complete compared to ISAR measured skin SST. The objectives of this study are to quantify bulk-skin SST differences and to derive accurate representations of skin temperature from bulk SST for further oceanographic and atmospheric studies relating to CASPER-East. A total of 2123 quality-controlled measurements of bulk and skin SST are considered in this analysis. Average bulk-skin SST difference estimated from the quality controlled data points during CASPER was found to be 0.4°C. Most of the time (~98%) during CASPER, the skin SST was cooler than bulk SST.

In this analysis, the variability of bulk-skin SST differences are shown to have a strong dependence on wind speed, and at wind speeds lower than 4 m s^{-1}, bulk-skin SST difference varies diurnally. To correct the bulk SST for cool skin and warm layer effects, a three-step correction method is employed. Initially, the bulk-skin

SST difference data are separated into low wind (<4 m s^{-1}) and high wind (>4 m s^{-1}) cases. Wind speed dependence on bulk-skin SST difference for low-wind and high-wind cases are then quantified separately using quadratic and linear least squares fits, respectively. Additionally, a sine fit is used to quantify the diurnal signal in the bulk-skin SST difference for low wind speed cases after it has been corrected for wind speed dependence. Finally, a linear fit is employed to quantify the increase in bulk-skin SST difference with net longwave radiation flux. This method significantly reduces the mean bulk-skin SST difference to nearly 0°C from its original value of 0.4°C. The error correction scheme seems to be effective for the CASPER-East data.

Comparison of bulk-skin SST difference observations with different models shows that the cool skin and warm layer model by *Fairall et al*. [1996] used in the COARE bulk flux algorithm [*Fairall et al*., 2003] matches well in the moderate wind regime ($\sim$3 to $\sim$7 m s^{-1}). Parameterizations based solely on wind speed proposed by *Donlon et al*. [2002] and *Minnett et al*. [2011] underestimate the observed bulk-skin SST difference. However, similar to the *Donlon et al*. [2002] and *Minnett et al*. [2011] parameterizations, the present observations of bulk-skin SST difference also follow an exponential fit for wind speeds greater than 2 m s^{-1}, but employ a different set of model coefficients.

Acknowledgments
CASPER is funded by the Office of Naval Research (ONR) under its Multidisciplinary University Research Initiative (MURI) program, grant N0001416WX00469, under project managers Daniel Eleuterio and Steve Russell. Data used for this study are available at https://workspace.axiomdatascience.com/group/282520/projects.

References

Alappattu, D. P., Q. Wang, and J. Kalogiros (2016), Anomalous propagation conditions over eastern Pacific Ocean derived from MAGIC data, *Radio Sci.*, *51*, 1142–1156, doi:10.1002/2016RS005994.

Donlon, C. J., and I. S. Robinson (1997), Observations of the oceanic thermal skin in the Atlantic Ocean, *J. Geophys. Res.*, *102*(C8), 18,585–18,606.

Donlon, C. J., P. J. Minnett, C. Gentemann, T. J. Nightingale, I. J. Barton, B. Ward, and J. Murray (2002), Toward improved validation of satellite sea surface skin temperature measurements for climate research, *J. Clim.*, *15*, 353–369.

Donlon, C. J., et al. (2007), The global ocean data assimilation experiment high-resolution sea surface temperature pilot project, *Bull. Am. Meteorol. Soc.*, *88*, 1197–1213.

Donlon, C. J., I. S. Robinson, M. Reynolds, W. Wimmer, G. Fisher, R. Edwards, and T. J. Nightingale (2008), An infrared sea surface temperature autonomous radiometer (ISAR) for deployment aboard volunteer observing ships (VOS), *J. Atmos. Oceanic Technol.*, *25*, 93–113, doi:10.1175/2007JTECHO505.1.

Fairall, C., E. Bradley, J. Godfrey, G. Wick, J. Edson, and G. Young (1996), Cool-skin and warm-layer effects on sea surface temperature, *J. Geophys. Res.*, *101*(C1), 1295–1308.

Fairall, C., E. Bradley, J. Hare, A. Grachev, and J. Edson (2003), Bulk parameterization of air–sea fluxes: Updates and verification for the COARE algorithm, *J. Clim.*, *16*, 571–591, doi:10.1175/1520-0442(2003)016<0571:BPOASF>2.0.CO;2.

Frederickson, P. A. (1994), The effect of infrared sea surface temperature measurements on evaporation duct height estimation, technical report, Naval Postgraduate School, Monterey, Calif. [Available at http://hdl.handle.net/10945/28715.]

Gentemann, C. L., and P. J. Minnett (2008), Radiometric measurements of ocean surface thermal variability, *J. Geophys. Res.*, *113*, C08017, doi:10.1029/2007JC004540.

Gentemann, C. L., P. J. Minnett, and B. Ward (2009), Profiles of ocean surface heating (POSH): A new model of upper ocean diurnal warming, *J. Geophys. Res.*, *114*, C07017, doi:10.1029/2008JC004825.

Hanafin, J. A. (2002), On sea surface properties and characteristics in the infrared, PhD thesis, University of Miami, Miami, Fla.

Hanafin, J. A., and P. J. Minnett (2001), Profiling temperature in the sea surface skin layer using FTIR measurements, in *Gas Transfer at Water Surfaces, Geophys. Monogr. Ser.*, edited by M. A. Donelan et al., pp. 161–166, AGU, Washington, D. C.

Horrocks, L. A., B. Candy, T. J. Nightingale, R. W. Saunders, A. O'Carroll, and A. R. Harris (2003), Parameterizations of the ocean skin effect and implications for satellite-based measurement of sea-surface temperature, *J. Geophys. Res.*, *108*(C3), 3096, doi:10.1029/2002JC001503.

Lukas, R. (1989), Observations of air-sea interaction in the western Pacific warm pool during WEPOCS, paper presented at the Western Pacific International Meeting and Workshop for TOGA COARE, Inst. Fr. De Rech. Sci. pour le Dev. En Coop. (ORSTOM), Noumca, New Caledonia.

Minnett, P. J. (2003), Radiometric measurements of the sea–surface skin temperature—The competing roles of the diurnal thermocline and the cool skin, *Int. J. Remote Sens.*, *24*, 5033–5047.

Minnett, P. J., M. Smith, and B. Ward (2011), Measurements of the oceanic thermal skin effect, *Deep Sea Res., Part II*, *58*, 861–868, doi:10.1016/j.dsr2.2010.10.024.

Niller, P. P., and E. B. Kraus (1977), One-dimensional models of the upper ocean, in *Modeling and Prediction of the Upper Layers of the Ocean*, edited by E. B. Kraus, pp. 143–172, Pergamon, New York.

Price, J. F., R. A. Weller, and R. Pinkel (1986), Diurnal cycling: Observations and models of the upper ocean response to diurnal heating, cooling, and wind mixing, *J. Geophys. Res.*, *91*(9), 8411–8427.

Robertson, J. E., and A. J. Watson (1992), Thermal skin effect of the surface ocean and its implications for CO_2 uptake, *Nature*, *358*, 738–740.

Saunders, P. M. (1967), Aerial measurements of sea-surface temperatures in the infrared, *J. Geophys. Res.*, *72*, 4109–4117, doi:10.1029/JZ072i016p04109.

Schluessel, P., W. J. Emery, H. Grassl, and T. Mammen (1990), On the bulk–skin temperature difference and its impact on satellite remote sensing of sea surface temperatures, *J. Geophys. Res.*, *95*(C8), 13,341–13,356.

Wang, Q., R. Burkholder, H. J. S. Fernando, D. Khelif, R. K. Shearman, and L. Shen (2015), Coupled air-sea processes and EM ducting research (CASPER), paper presented at the 19th AMS Conference on Air-Sea Interaction, Am. Meteorol. Soc., Phoenix, Ariz.

Ward, B. (2006), Near-surface ocean temperature, *J. Geophys. Res.*, *111*, C02004, doi:10.1029/2004JC002689.

Wilson, R. C., S. J. Hook, P. Schneider, and S. G. Schladow (2013), Skin and bulk temperature difference at Lake Tahoe: A case study on lake skin effect, *J. Geophys. Res. Atmos.*, *118*, 10,332–10,346, doi:10.1002/jgrd.50786.

Zeng, X., and R. E. Dickinson (1998), Impact of diurnally-varying skin temperature on surface fluxes over the tropical Pacific, *Geophys. Res. Lett.*, *25*, 1411–1414.

Zeng, X., M. Zhao, R. E. Dickinson, and Y. He (1999), A multiyear hourly sea surface skin temperature data set derived from the TOGA TAO bulk temperature and wind speed over the tropical Pacific, *J. Geophys. Res.*, *104*(C1), 1525–1536, doi:10.1029/1998JC900060.